Tutor/s
Dr. Raimundo Gargallo Gómez
Departament d'Enginyeria Química i Química Analítica

Grau de Química

Treball Final de Grau

Study of the interaction of fluorescent dyes with several DNA structures.
Estudi de la interacció de marcadors fluorescents amb diverses estructures de l'ADN.

Ona Raset Vidal

JANUARY 2025

UNIVERSITAT DE BARCELONA
B:KC Barcelona Knowledge Campus
Campus d'Excel·lència Internacional

Hi ha una força motriu més poderosa que el vapor, l'electricitat i l'energia atòmica: la voluntat.

Albert Einstein

Primerament, vull donar les gràcies al meu tutor, Raimundo Gargallo, pel seu suport, atenció i per ensenyar-me tots els coneixements acadèmics necessaris per poder realizar aquest projecte.

També m'agradaria agrair a la meva familia i amics per la paciencia i el recolzament que han mostrat.

REPORT

IDENTIFICATION AND REFLECTION ON THE SUSTAINABLE DEVELOPMENT GOALS (SDG)

The Sustainable Development Goals (SDGs) consist of a set of 17 global goals adopted by the United Nations in 2015 as a part of the 2030 Agenda for Sustainable Development. This agenda aims to make a universal call to eradicate poverty, protect the planet, and ensure that all people enjoy peace and prosperity by 2030. The SDGs encompass a wide range of areas, including health, education, climate change, gender equality, innovation, and social justice.

This project contributes primarily to SDG 3: Good Health and Well-being, and SDG 9: Industry, Innovation, and Infrastructure.

SDG 3: Good Health and Well-being

This goal seeks to ensure healthy lives and promote well-being for all. Specially, Target 3.4 focuses on reducing premature mortality from non-communicable diseases by one-third through prevention and treatment. The project aligns with this goal by studying fluorescent ligands like R9, which stabilize G-quadruplex DNA structures. These structures are crucial for regulating telomerase, and enzyme associated with the growth of cancer cells. Therefore, the findings have the potential to contribute to the development of new, targeted therapies against cancer. The other DNA structures studied were also targeted for innovation to expand the research into new directions.

SDG 9: Industry, Innovation, and Infrastructure

The project also strengthens scientific and technological capacities, aligning with Target 9.5, which focuses on enhancing scientific research and technological capabilities in industrial sectors. The project employs advanced techniques, including fluorescence spectroscopy, circular dichroism, and high-performance liquid chromatography (HPLC). The result confirm that the R9 ligand boosts the thermal stability of G-quadruplex structures, opening up potential uses for telomerase inhibition in cancer treatments. Additionally, the reactivation of an old HPLC system highlights a sustainable approach to research by minimizing the need for new equipment and maximizing the use of existing resources.

Expanding the scope of the project could yield several significant outcomes:

- The stabilization of G-quadruplex could be applied in specific treatments to regulate cancer-related processes.
- Research could advance toward the development of less toxic and more sustainable fluorescent biomarkers for medical applications.

In summary, this project not only advances the understanding of complex DNA structures and their interactions with ligands but also aligns with key SDG goals by promoting global health, scientific innovation, and sustainability in research.

CONTENTS

1. SUMMARY

This project studies the interaction of the fluorescent ligand R9 with various DNA structures, such as G-quadruplex, duplex, hairpin, and i-motif, using techniques like fluorescence spectroscopy, circular dichroism, UV-Vis spectroscopy, and high-performance liquid chromatography (HPLC). The main objective is to characterize the binding properties and structural effects that R9 induces in these DNA structures.

The result shows that the R9 ligand binds to all the studied DNA structures, even though the strength of this interaction depends on the shape of each structure. In particular, the parallel G-quadruplex Pu22T14T23 stands out for its high affinity, which is evidenced by increased fluorescence, changes in UV-Vis absorption spectra, and a significant increase in thermal stability. Circular dichroism data suggest that, in G-quadruplex, R9 binds externally through π-π stacking between the nitrogenous bases and the ligand, as well as electrostatic interactions. In the case of the duplex H28, the ligand intercalates between the strands.

Thermal denaturation measurements indicate that R9 enhances the stability of most DNA structures, raising their melting temperatures (Tm). This effect is clearly seen in the parallel G-quadruplex Pu22T14T23, which exceeds 95 ºC in the presence of R9. However, in hybrid structures like IDJ1 (which combines an i-motif and a hairpin), the effect of the ligand varies more, making some structural components less stable.

Finally, the project included the set up of an HPLC system that had not been used for years. The restarting of the HPLC system confirmed the functionality of the equipment, although the separation of DNA structures was not optimal with the column used.

In summary, this study demonstrates that the R9 ligand can stabilize non-canonical DNA structures, particularly G-quadruplex. This makes it a good candidate for studies on telomerase inhibition in cancer cells.

Keywords: DNA, R9 ligand, spectroscopy, interactions, thermal stability.

2. RESUM

Aquest projecte estudia la interacció del lligand fluorescent R9 amb diverses estructures d'ADN, com el G-quàdruplex, el dúplex, les forquetes i l'i-motif, mitjançant tècniques com l'espectroscòpia de fluorescència, el dicroisme circular, l'espectroscòpia UV-Vis i la cromatografia líquida d'alta resolució (HPLC). L'objectiu principal és caracteritzar les propietats d'unió i els efectes estructurals que el R9 indueix en aquestes estructures d'ADN.

Els resultats mostren que el lligand R9 s'uneix a totes les estructures d'ADN estudiades, tot i que la força d'aquesta interacció depèn de la forma de cada estructura. En particular, el G-quàdruplex paral·lel Pu22T14T23 destaca per la seva alta afinitat, la qual cosa es manifesta en una major fluorescència, alteracions en els espectres d'absorció UV-Vis i un notable increment en la seva estabilitat tèrmica. Les dades de dicroisme circular confirmen que, en els G-quàdruplex, el R9 s'uneix externament mitjançant apilaments π-π entre les bases nitrogenades i el lligand, a més d'interaccions electrostàtiques. En el cas del dúplex, l'H28, el lligand s'intercala entre les cadenes.

Les mesures de desnaturalització tèrmica indiquen que el R9 millora l'estabilitat de la majoria d'estructures d'ADN, elevant-ne les temperatures de fusió (Tm). Aquest efecte es veu clarament en el G-quàdruplex paral·lel Pu22T14T23, que supera els 95 ºC en presència de R9. No obstant això, en estructures híbrides com l'IDJ1 (que combina un i-motif i una forqueta), l'efecte del lligand canvia més, fent que alguns components estructurals siguin menys estables.

Finalment, el projecte va incloure la posada en marxa d'un sistema HPLC que no s'havia utilitzat durant anys. El reinici del sistema HPLC va permetre confirmar la funcionalitat de l'equip, encara que la separació d'estructures d'ADN no va ser òptima amb la columna utilitzada.

En resum, aquest estudi demostra que el lligand R9 pot estabilitzar estructures no canòniques d'ADN, especialment els G-quàdruplex. Això el fa un bon candidat per a estudis sobre la inhibició de la telomerasa en cèl·lules canceroses.

Paraules clau: ADN, lligand R9, espectroscòpia, interaccions, estabilitat térmica.

3. INTRODUCTION

DNA is a chain of nucleotides, which are the basic structural units of this molecule. Each nucleotide is made up of three parts:

1. A five-carbon sugar called deoxyribose, which forms the central framework of the nucleotide.
2. A nitrogenous base attached to the C1' atom of the deoxyribose. This base can be adenine (A), guanine (G), cytosine (C), or thymine (T). At pH 7, all these bases are electrically neutral. However, at moderately acidic pH, adenine (A) and cytosine (C) become protonated, acquiring a positive charge (acting as bases), while at moderately basic pH, guanine (G) and thymine (T) lose protons, acquiring a negative charge (acting as acids). These bases play a key role in DNA's ability to store genetic information.
3. A phosphate group, which links the nucleotides into the chain, remains deprotonated under most conditions, except at very acidic pH.

In the DNA strand, the phosphate group attached to the 5' carbon of one deoxyribose forms a bond with the 3' carbon of the deoxyribose in the next nucleotide. This linkage, called a phosphodiester bond, creates a repeating sugar-phosphate backbone. The backbone establishes a well-defined directionality in the DNA strands, with one end referred to as the 5' end (where the phosphate group is free) and the other as the 3' end (where a hydroxyl group is exposed on the sugar). [1]

DNA can adopt different conformation (Figure 1), the most common and stable topological form being B-DNA. This structure is a dextrorotatory double helix in which the strands are linked by bonds between the nitrogenous bases according to Watson and Crick's pairing rules: A is paired with T and G with C. The stability of this structure is mainly due to the stacking of the nitrogenous bases [2].

In environments with certain ionic concentrations, DNA can adopt the A-DNA conformation [3]. This form is characterised by a particular alignment of the adenines, resulting in a larger helix diameter and a shorter turn length compared to B-DNA.

Under the same conditions, the Z-DNA form can also appear. In this conformation, the helix turns in a levorotatory (the opposite of dextrorotatory) direction and has a zigzag-shaped sugar-phosphate backbone due to the alternating orientation of the carbohydrate groups [4].

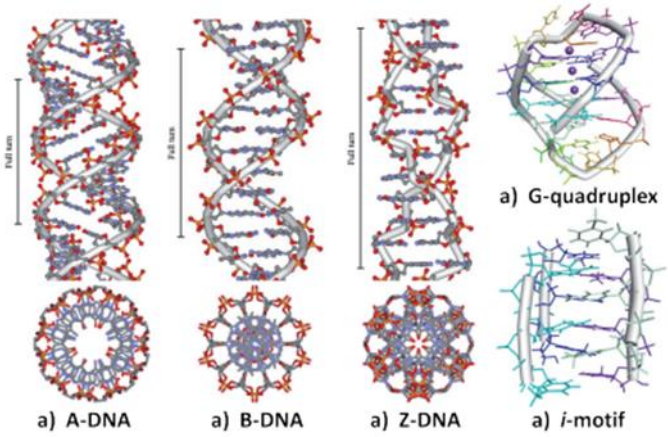

Figure 1: Different structures of DNA. [1]

In addition to B-DNA, A-DNA and Z-DNA, DNA can adopt other special conformations, such as hairpin, triplex (H-DNA), G-quadruplex and i-motif structures, among others. These structures will be explained in more detail below.

3.1. G-QUADRUPLEX

G-quadruplexes are structures made up of DNA or RNA that are organized within guanine-rich sequences. They can be generated by the folding of a single chain (intramolecular) or by the union of two (bimolecular) or four (tetramolecular). Guanine bases are bonded together by hydrogen bonds. Specifically, the guanines organize in groups of four to form a guanine tetrad, which is stabilized by hydrogen bonds known as Hoogsteen bonds. These tetrads can stack vertically on top of one another, forming three-dimensional structures known as G-quadruplex. This stacking is further stabilized by π-π interactions between the aromatic rings of the guanine bases.

These structures present a great topological diversity, which depends on factors such as the orientation of the chains, the size and sequence of the loops, and chemical conditions, such as the presence of specific cations.

Guanine in G-quadruplexes can adopt two different conformations depending on the orientation of their glycosidic bond, as shown in Figure 2. When the guanine base and the glycosidic bond are on the same side, it is called *syn* conformation. If they are on opposite sides, it is called *anti* conformation.

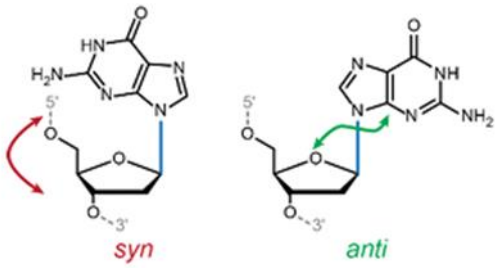

Figure 2: Syn and anti glycosidic bond angles of guanosine. [5]

The orientation of the strings defines whether the structure is parallel or antiparallel. In parallel structures, all chains have the same polarity, following the 5' to 3' direction of the phosphate backbone. In this case, the guanines all adopt the *anti*-conformation, and the chains are oriented in the same direction. On the other hand, in antiparallel structures, at least one of the chains is antiparallel with respect to the others, which generates a combination of *anti* and *syn* conformations. There is also the hybrid structure, where three chains are oriented in one direction and the fourth in the opposite [5]. In Figure 3, the described structures can be seen.

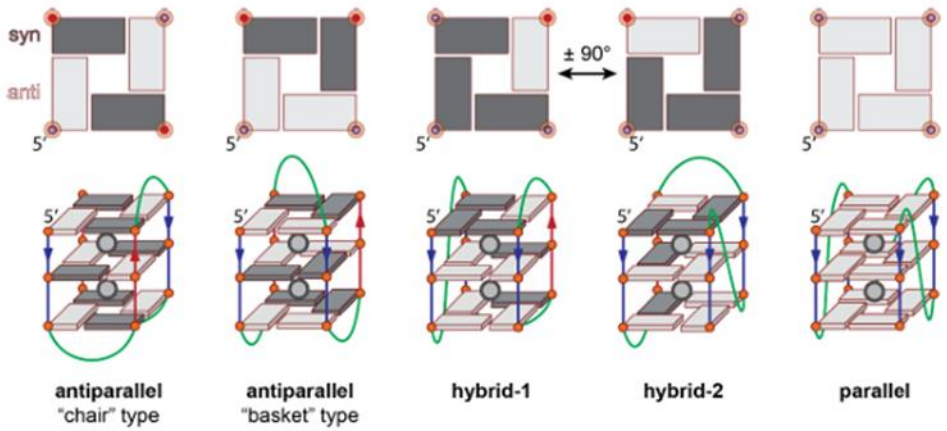

Figure 3: The image shows G-quadruplex structure with different types of loops. The rectangles represent the guanines, and their distinct colours indicate the syn or anti position of each guanine. The small spheres correspond to cations. In parallel conformations, the loops are helical and referred to as propeller loops. In antiparallel structures, the loops can be lateral, connecting adjacent strands, or diagonal, linking opposite strands. [5]

Apart from polarity, G-quadruplex structures include loops, which are regions of nucleotides (thymine, adenine, and cytosine) located between guanine tetrads. In vertebrate telomeres, the sequence consists of a continuous repetition of guanine-rich segments. However, in other non-telomeric genomic regions, guanines are separated by loops. In parallel structures, the connecting loops link the lower tetrad to the upper one, forming helical loops referred to as propeller loops. In antiparallel structures, two types of loops can be identified [6]:

- Lateral loops: These connect adjacent guanine strands situated on the same face or opposite faces.
- Diagonal loops: These connect opposite strands, requiring adjacent strands to alternate between parallel and antiparallel orientations.

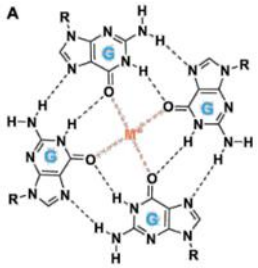

Figure 4: Chemical structure tetrad. [5]

The stability of G-quadruplexes depends on the presence of monovalent cations. These ions coordinate with the oxygen atoms (O6) of the guanines, positioning themselves in the central channel formed by the tetrads (Figure 4). Among these cations, potassium (K^+) is the most effective at stabilizing the structure due to its ability to form a symmetrical tetragonal bipyramidal configuration with the oxygen atoms. The preference for cations follows the order: $K^+ > Na^+ > Li^+$, with potassium being the most efficient stabilizer. [6] [7]

G-quadruplexes play a prominent role in genomic regulation at the gene promoter level and chromosome stability. These structures can be found near the promoter regions of some genes. Pu22T14T23, one of the G-quadruplex structures to be studied, is in these regions.

Telomeres consist of duplex DNA repeats (TTAGGG) and a single-stranded guanine-rich tail at the 3' end. G4 structures can protect telomeres. Telomerase is a reverse transcriptase enzyme that replicates repetitive segments at the 3' end of telomeric DNA, which is found at high levels in cancers. One way to stop telomerase has been to place a molecule at the telomeric end forming a stable G4 structure, which makes telomerase unable to act.

To study more carefully the action of the G4 structure at the gene promoter and telomeres, we want to find small molecular ligands that bind to G4, and, therefore, study ligand specificity within the quadruplexes. [8]

3.2 I-MOTIF

The G-quadruplex structure, which contains guanine-rich regions of DNA, has been discussed above. Cytosine-rich regions can also be found, which can form a folded structure known as i-motif. This structure is formed by two parallel, right-handed helix DNA duplexes, and contains a neutral cytosine (C) and a protonated cytosine (C^+) at nitrogen 3 (N3), linked by three hydrogen bonds (Figure 5). These bases are intercalated in an antiparallel way to each other. [9] [10]

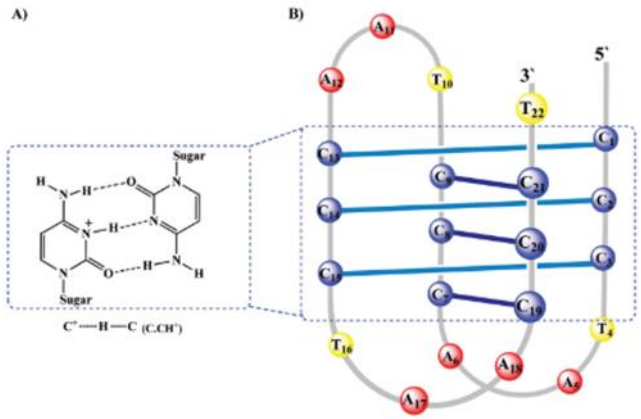

Figure 5: Folding structure of human telomeric DNA i-motif: (A) C·C⁺ base pair, (B) intramolecular structure of human telomeric DNA i-motif 5'- d[(CCCTAA)$_3$CCCT]-3'. [10]

In vitro studies have shown that this type of structure is stable only at pH values below 7 under physiological conditions of temperature and ionic strength. This is because the pK_a of the conjugated acid of cytosine is approximately 4.5 at 25 ºC and 0.1 M ionic strength [11]. At neutral pH, the protonated form of cytosine (C^+) is present in very low concentrations, making the stabilization of the structure through protonated cytosines unlikely.

The i-motif structure can be intramolecular, where the cytosine regions are located a single chain; or intermolecular, where the cytosine stretches are on two or four independent chains. [9]

3.3 HAIRPIN

An alternative form of non-B-DNA conformation is the hairpin structure, characterized by base pairing within a single strand (intramolecular double-stranded helix). These structures consist of two main components:

1. The stem, where base pairing occurs.
2. The loop, formed by a sequence of nucleotides that are either unpaired or do not follow Watson-Crick pairing rules.

The properties of the loop, such as its radius, stem length, or sequence type, can vary depending on the bases that compose it. [12]

There are two primary mechanisms for the formation of hairpin structures in DNA:

1. From Single-Stranded DNA (ssDNA): In the single-stranded state, DNA is not merely an inert intermediary; rather, it can fold into secondary structures. These structures are essential because they are recognized by proteins involved in processes such as site-specific recombination, transcription, and replication. [13]
2. From Double-Stranded DNA (dsDNA): In this case, hairpin structures adopt a cruciform shape, consisting of two opposing hairpins. These are formed through base pairing within the same helix from palindromic sequence.

A palindromic sequence in defined as a sequence of nucleic acids (in double-stranded DNA or RNA) that reads the same in one direction (e.g., 5' to 3') on one strand as it does in the same direction (5' to 3') on the complementary strand. [13]

Figure 6 shows the two discussed structures.

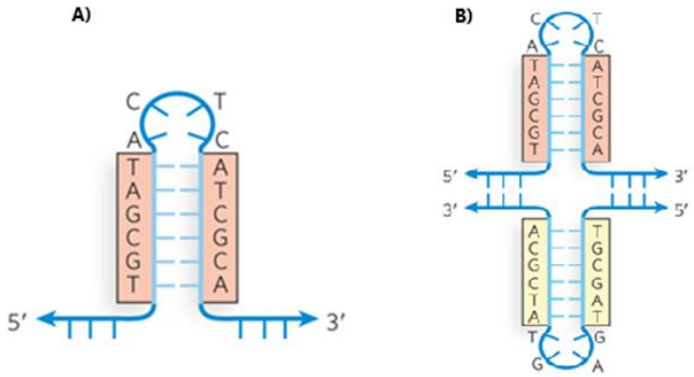

Figure 6: (A) Intramolecular hairpin structure. (B) Intermolecular cruciform structure.

3.4. R9 LIGAND

The growing need to advance research on DNA structures and processes has created a significant demand for the development of fluorescent biomarkers to enable the visualization of these interactions.[14]

In this context, fluorescent markers play a crucial role. These compounds can emit fluorescence when interacting with specific cellular components, making them indispensable tools for the visualisation of intracellular structures. Among the dyes used to label nucleic acids, cyanine dyes stand out for their ability to fluoresce only upon interaction with specific biomolecules, which minimises background signals and increases the accuracy of studies. In addition, they have advantages such as low toxicity, ease of handling and versatility for functional modifications. [15]

The marker selected for this study is the ligand known as “R9”, shown in the Figure 7, a compound belonging to the cyanine family. It has been synthesized by the research group of Dr. Aleksey Vasilev and Dra. Diana Cheshmedzhieva at the University of Sofia (Bulgaria). Its chemical name is (E)-1-(3-amino-3-oxopropyl)-4-((3-(3-(3-(3-(pyridin-1-io-1-yl)propyl)venzo[d]thiazol-2(3H)-ylidene)methyl)quinolin-1-io diiodide, and it is classified as a fluorogenic dye. This means that it emits fluorescence when interacting with specific biomolecules and is particularly useful for studying DNA.

R9 is a dicationic, asymmetric, monomethine cyanine dye composed of benzothiazolium and chloroquinoline terminals linked through propylpyridinium and aminooxopropyl functional side groups. An outstanding feature of this compound is its high selectivity towards GC-DNA versus AT-DNA base pairs.

The characteristic fluorescence of R9 is because, upon interaction with a biomatrix such as DNA, its chemical structure is rigidified. This change reduces the loss of energy in the form of heat, resulting in intense fluorescent emission. These properties make R9 an ideal marker for applications where specific visualisation of DNA is essential. [14]

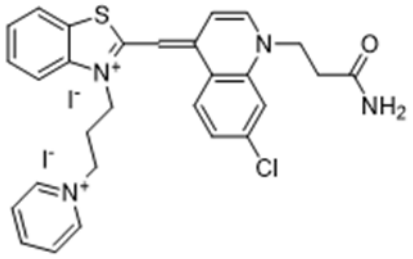

Figure 7: Structure of the R9 ligand.

4. OBJECTIVES

The main objective of this project is to study the interaction of the fluorescent ligand R9 with different DNA structures, such as the G-quadruplex, the duplex, the hairpin, and the i-motif. To achieve this, spectroscopic techniques will be employed, including molecular absorption, fluorescence, and circular dichroism.

Additionally, the aim is to reactivate an HPLC system that has been unused for years. In this context, different mobile phases will be investigated to determine the most suitable one for analysing DNA samples.

5. EXPERIMENTAL SECTION

5.1 REAGENTS AND SOLUTIONS

To carry out the experimental part of the project, the analytes were treated to be able to work with them. DNA solutions and the R9 ligand solution were prepared using a phosphate buffer with a pH of 7.4 obtained from Merck (St. Luis, MO, USA), KCl acquired from Merck, and Milli-Q® water from Millipore, USA. Both the DNA samples and the ligand contained 20 mM phosphate buffer, 50 mM KCl, and Milli-Q® water, maintaining the temperature at 20 ºC. Ligand R9, which was red in his solid state, was dissolved in DMSO, obtained from VWR CHEMICALS (Radnor, PA, USA), to reach a concentration of 1 mM, and the resulting solution was also red. All measurements were made with micropipettes, selecting the most suitable one for the required volume.

Below is the Table 1 summarizing the names of the analysed sequence, their respective nucleotide sequence, and the structures adopted by each:

Table 1: DNAs with their sequence and structure.

Name	Sequence (5' --> 3')	Expected structure
Pu22T14T23	TGA GGG TGG GTA GGG TGG GTA A	Parallel G-quadruplex
TBA	GG TT GG TGT GG TT GG	Antiparallel G-quadruplex
QDJ1	GGT TGG CGC GAA GCA TTC GCG GGT TGG	Antiparallel G-quadruplex hairpin junction
IDJ1	CCC GTT TCC TCG CGA AGC ATT CGC GCC CGT TTC CT	i-motif – hairpin junction
H28	AGG AAG GAA AAG TTTT CTT TTC CTT CCT	Intramolecular duplex
T25	T25	Unstructured strand

Figure 8 show the structures of Pu22T14T23, TBA, QDJ1, and IDJ1. The G-quadruplex can be observed in both Pu22T14T23 and TBA, although Pu22T14T23 is parallel while TBA is antiparallel. Additionally, the difference between QDJ1 and IDJ1 can be seen, as QDJ1 contains a duplex with a G-quadruplex, whereas IDJ1 contains a duplex with an i-motif.

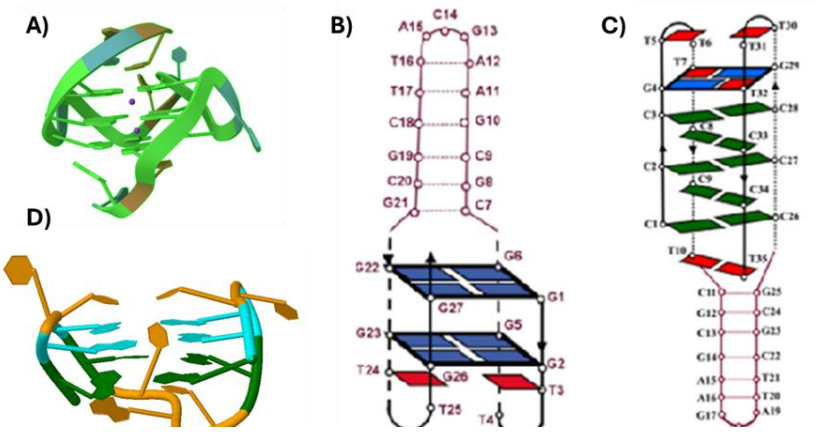

Figure 8: (A) Structure of Pu22T14T23 (B) Structure of QDJ1 [22] (C) Structure of IDJ1 [23] (D) Structure of TBA. The structures (A) and (D) have been built with the Molecular Viewer toolbox for MATLAB® from the corresponding .pdb files

5.2 TECHNIQUES AND INSTRUMENTATION

5.1.1 Molecular absorption spectrometry

UV-Vis spectrometry is based on measuring a sample's ability to absorb light within the ultraviolet and visible range of the electromagnetic spectrum, typically between 200 and 800 nm. The basic principle of the UV-Vis spectrophotometer is rooted in Lambert-Beer's law, which states that the absorbance of a substance is directly proportional to its concentration and the optical path length.

This instrument consists of a light source, a monochromator to select the desired wavelength, a sample cell, and a detector. The light passes through the sample, and the detector measures the intensity of the light before and after passing through the sample, allowing de absorbance to be calculated.

A model 8453 spectrophotometer (Agilent Technologies, Germany) equipped with a Peltier temperature control system was used. Measurements were performed over a wavelength range of 350 to 700 nm. Absorbance spectra were obtained using the same instrument, which was equipped with a diode array detector and blank correction. The temperature of the cuvette, with a 1 cm optical path length (Hellma, Germany) was regulated using the Agilent 89090A Peltier device.

5.1.2 Fluorescence spectroscopy

The fluorescence spectrophotometer is used to analyse the fluorescence of a sample. This type of spectroscopy is based on the ability of certain molecules to emit lower-energy light (usually visible light) after being excited by a beam of light.

The operating principle of the fluorescence spectrophotometer involves the absorption of photons by the molecules in the sample, which excites their electrons to a higher energy state. Subsequently, these electrons return to their ground state, emitting photons in the process. The wavelength of the emitted light is characteristic of the substance and can be used for its identification and quantification.

The fluorescence spectrophotometer consists of several components: a light source, a monochromator to select the excitation wavelength, a sample cell, and a detector placed at a 90º angle to the excitation light to avoid contamination of the results. This detector measures the intensity of the emitted fluorescent light, allowing an emission spectrum to be obtained.

Fluorescence spectra were acquired using an Aminco-Bowman series 2 spectrofluorometer at room temperature. The excitation wavelength was set at 10 nm intervals within the range 400 to 600 nm, while the emission wavelength was recorded in the range 500 to 700 nm, with a sensitivity of 700 V.

5.1.3 Circular dichroism spectroscopy

Circular Dichroism (CD) is a spectroscopic technique that measures the difference in the absorption of right-and left-circularly polarized light as it passes through chiral molecules. This difference arises from the asymmetric three-dimensional structure of chiral molecules, which interact differently with light depending on its polarization. CD provides key information about the structural properties of molecules, especially in biopolymers such as DNA.

The circular dichroism spectrometer consists of a light source, a polarize to generate circularly polarized light, a sample cell, and a detector. The circularly polarized light interacts with the sample, and the detector measures the difference in absorbance between the two polarizations. [16]

The spectrophotometer used was the JASCO J815 model (Japan Spectroscopy Company), equipped with a Peltier temperature control. We used Spectra Manager software to carry out the measurements.

5.1.4 High-Performance Liquid Chromatography

High-Performance Liquid Chromatography (HPLC) is an advanced analytical technique used to separate, identify, and quantify components of a mixture. It uses high pressure to push solvents through a column packed with fine particles, which enhances separation efficiency. The sample is introduced into a flow of mobile phase (solvent or buffer) that carries it to the column, which contains a stationary phase, typically small particles of silica or polymer material. The different compounds in the sample interact with the stationary phase in various ways, causing them to move at different speeds. Compounds with a higher affinity for the stationary phase will be delayed more, while those with lower affinity will move faster, allowing their separation. [17]

The HPLC equipment used belongs to the Water brand and consist of the following modules: a 600 Controller pump, a 717 Plus injector, and a 996 photodiode array detector. The chromatographic column employed was the Walters Atlantis T3, 100 Å ,5 µm, 2.1x150 mm, a C18 reverse-phase column. The system was controlled and managed using Empower software, also from Waters.

5.2. EXPERIMENTAL PROCEDURE

In the section Reagents and Solutions, it was explained how the DNA and ligand samples were treated to carry out the different experimental procedures. Next, the corresponding procedure for each instrument is detailed.

5.2.1. Molecular absorption spectrometry

An R9 solution was prepared at a concentration of 1.5 µM in a total volume of 400 µL. Similarly, DNA solutions were prepared at a concentration of 50 µM in a total volume of 70 µL. The titrations were performed by gradually adding 2.5 µL of the DNA solution to the R9 solution. This process continued until a total of 40 µL of DNA had been added. The titration process was carried out for all DNA samples.

5.2.2. Fluorescence spectroscopy

The samples used contained DNA and R9, and their preparation did not require specific conditions. The solution obtained from the titrations performed with the UV-Vis spectrophotometer were used. The final concentrations were 4.55 µM for DNA and 1.36 µM for R9.

5.2.3 Circular dichroism spectroscopy

To perform the circular dichroism measurements, two types of solutions were prepared: one containing only DNA and another containing DNA and R9. For all DNA samples, 1 mL of solution was prepared with a DNA concentration of 2 µM, using a medium composed of 20 mM phosphate buffer, 50 mM KCl, and Milli-Q® water, consistent with the conditions used for other instruments. For the solutions containing both DNA and R9, the concentrations were adjusted to maintain a 1:3 ratio of DNA to R9. As a result, the final concentrations were 2 µM for DNA and 6 µM for R9.

Initially, measurements were performed on both the DNA-only solutions and the DNA-R9 solutions.

Subsequently, we performed thermal denaturation measurements by increasing the temperature. Each DNA sample has a specific temperature range, although generally a range of 5 ºC to 95 ºC was covered. The temperature was increasing at a rate of 1 ºC/min, with a waiting time of 60 seconds. Ellipticity was monitored at the wavelength corresponding to the maximum ellipticity observed in the initial measurement. These measurements were performed exclusively for Pu22T14T23, H28, QDJ1 and IDJ1, as well as for their respective mixtures with R9.

Finally, we performed two titrations with Pu22T14T23 and H28, starting with a 2 µM DNA solution and adding 2 µL of R9 at 1 mM, until a final ratio of 10:1 (R9: DNA) was reached.

5.2.4. High-Performance Liquid Chromatography

This instrument has not been in use for several years, and my task was to restore it to full functionality. To achieve this, I studied its components, operation, and associated software.

Initially, a reference standard, anthracene, was used with a mobile phase composed of water and acetonitrile (ACN) in a 25:75 ratio. The concentration of anthracene was 100 mg/L in acetonitrile. Next, two mobile phase solutions were prepared based on previous study [18], since the analyte was also DNA. The prepared solutions were: 5% ACN in TEAA (triethylamine acetate) and 70 % ACN in TEAA. Several tests were conducted using 10 µM DNA samples, varying the rations of both mobile phase solutions.

Finally, the mobile phase was changed to a mixture of TEAA 0.1 M and ACN. The optimal combination was found to be 60:40 (TEAA: ACN).

As previously mentioned, a C18 reverse-phase column was used. In all measurements, the flow rate was maintained at 0.25 mL/min, with an injection volume of 10 µL. All tests were conducted at room temperature.

5.2.4 Data Processing

To extract the information from the instruments, data processing had to be performed. This process was carried out using MATLAB® and Microsoft Excel®. MATLAB® version R2024b was used, which has been useful for creating the graphs for this project. Microsoft Excel® was applied to perform the preliminary calculations needed to prepare the solutions required for the experiments, as well as to process the HPLC data and create the corresponding diagrams.

In the results discussion section, for the analysis of denaturation temperature (T_m), the sigmoidal equation was used, which allows for the interpretation of this temperature. In the Equation 1, the parameter "c" represents the T_m. Some structures showed only one transition, as seen in the first equation. In the case of the i-motif, two transitions were observed, corresponding to the second equation. To obtain the sigmoidal graph (Figure 16), the *cftool* tool in MATLAB® was used.

$$a + \frac{b}{1 + e^{-\frac{(x-c)}{d}}}$$

$$\left(a1 + \frac{b1}{1 + e^{-\frac{(x-c1)}{d1}}}\right) + \left(a2 + \frac{b2}{1 + e^{-\frac{(x-c2)}{d2}}}\right)$$

Equation 1: Sigmoidal function. The parameter "c" indicates the midpoint of the transition, i.e., the melting temperature (T_m). The first equation corresponds to a single transition, and the second to two transitions.

6. RESULTS AND DISCUSSION

In this section, the results obtained from the measurements described above will be presented and discussed.

6.1 MOLECULAR FLUORESCENCE SPECTROSCOPY

The main objective of the fluorescence measurements was to determine whether the ligand, previously identified as fluorogenic, emitted fluorescence when interacting with DNA. Three-dimensional plots showing the fluorescence generated by the ligand upon interaction with the different DNA structures are presented in the Figure 9.

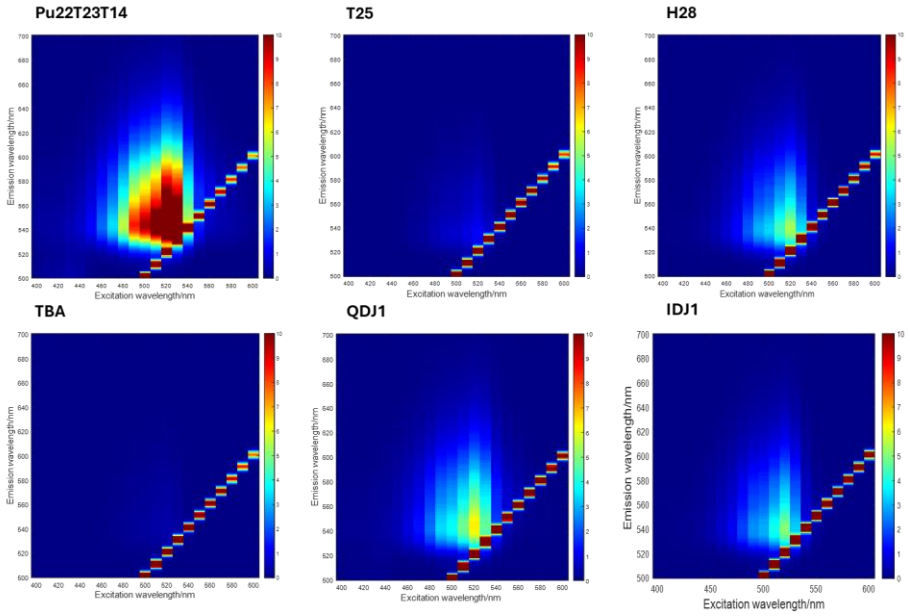

Figure 9: Emission *vs*. Excitation Wavelength of fluorescence of DNA samples with R9.

These plots represent excitation wavelengths (x-axis) versus emission wavelengths (y-axis), while fluorescence intensity is indicated by a colour gradient. In all plots, a characteristic diagonal line is observed in the excitation-emission matrices, known as Rayleigh scattering. This phenomenon occurs when incident light interacts elastically with molecules, scattering at the same wavelength as the excitation light, with no loss of energy.

Table 2 summarizes the excitation and emission wavelength data, as well as the maximum fluorescence intensity recorded for each DNA interaction with the R9 ligand. An analysis of the results reveals that the interaction between Pu22T14T23 and R9 produces fluorescence significantly more intense than in the rest of the samples, although the other DNA structures also fluorescence with lower intensity. It is important to note that the emission wavelengths are longer than the excitation wavelengths, which is explained by the processes associated with the transition of an electron to a higher energy level, since the wavelength is inversely proportional to the energy, and when a molecule absorbs radiation, an electron is excited to a higher level. However, during the relaxation process, the electron returns to the ground state with a partial loss of energy, resulting in a lower energy emission and, therefore, a longer wavelength for fluorescence.

In this case, the emission wavelength is in the range 539-543 nm, indicating that the samples emit green light when fluorescing.

Table 2: Excitation and emission wavelength, fluorescence intensity of DNA sample

DNA	λ excitation [nm]	λ emission [nm]	Fluorescence intensity
Pu22T14T23	530	543	15.3
TBA	520	539	0.4
QDJ1	520	541	6.4
IDJ1	520	539	5.1
H28	520	539	5.4
T25	520	534	1.2

From the fluorescence results, it is confirmed that there is interaction between DNA and the R9 ligand, but there is insufficient information to determine how these interactions vary for different DNA structures. Therefore, further experiments were carried out with other instruments to obtain complementary data and deepen the analysis.

6.2. MOLECULAR ABSORPTION UV-VIS SPECTROSCOPY

As described above, titrations of R9 ligand with different DNA samples were performed using a UV-Vis spectrophotometer. The resulting graph shows absorbance as a function of wavelength.

In the initial graph, the dark blue curve represents the spectrum of R9 in the absence of DNA. This spectrum allows us to identify the wavelength of maximum absorbance for the ligand when no DNA is present, a parameter that remained consistent across all titrations with the different DNA types, corresponding to a value of 509 nm. The graphs for the titrations with Pu22T14T23 and T25 DNA, selected for their clearly differentiated behaviour, are presented below (Figure 10).

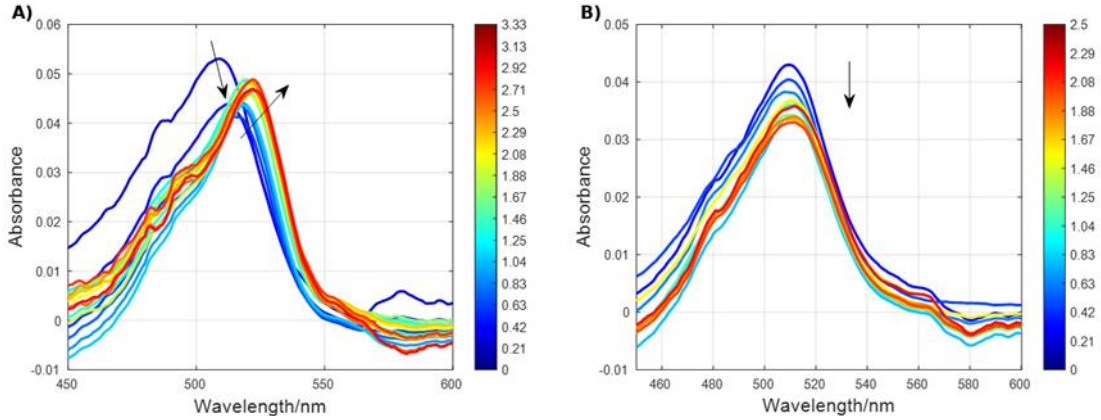

Figure 10: Absorbance *vs.* Wavelength of titration of (A) Pu22T14T23 with R9 and (B) T25 with R9. Initial R9 concentration was 1.5 micromolar. Experiments carried out at 20 ºC. Numbers at the colour bar indicate the changes associated with increasing DNA concentrations.

For Pu22T14T23 DNA, a decrease in the intensity of the absorbance maximum is observed, a phenomenon known as hypochromic shift. This term refers to a reduction in absorbance at a specific wavelength, usually caused by molecular interaction or structural changes. In addition, a shift of the absorbance maximum towards longer wavelengths is observed as the DNA concentration increases, a phenomenon called bathochromic shift. This behaviour is related to a change in the electronic environment of the ligand due to its specific interaction with DNA. In contrast, the graph for T25 DNA does not show a wavelength shift, as this DNA is a single strand that does not generate significant changes with the ligand's electronic environment. However, a small hypochromic shift is observed, which is evidence that there is a weak interaction between the ligand and the DNA.

Table 3 presents the absorbance maxima measured when the concentration of R9 and DNA is at a 3:1 molar ratio. It also includes the wavelength shift relative to the maximum absorbance of the R9 ligand in the absence of DNA, as well as the percentage of hypochromic shift observed in each titration.

Table 3: Maximum wavelength at 3:1 (R9: DNA) molar ratio, the value of Δλ and the hypochromic percentage of the DNA samples.

DNA	λ [nm]	Δλ [nm]	Hypochromicity [%]
-	509	0	-
Pu22T14T23	522	13	-11.7
TBA	512	3	-40.6
QDJ1	521	12	-22.8
IDJ1	520	11	-10.9
H28	517	8	-25.5
T25	512	3	-16.7

The concepts of hypochromic and bathochromic shifts, which are key to interpret the interactions between the R9 ligand and the different DNA structures, have been described before. In all the structures studied, a decrease in absorbance is observed, which translates into a percentage of hypochromic shift. This negative percentage reflects this decrease and is indicative of an interaction between the ligand and the DNA.

Regarding the bathochromic shift, it is observed in most of the titrations performed. However, in case of T25, this phenomenon is almost imperceptible. This is because, in T25, the interaction between the ligand and the DNA is probably exclusively electrostatic. The positively charged R9 ligand, due to its protonated amines, interacts with the negatively charged phosphate groups of the DNA. These electrostatic interactions are the only form of interaction that occurs between the ligand and T25, which explains the absence of a significant wavelength shift.

On the other hand, in structures such as the G-quadruplex, present in Pu22T14T23 and TBA, in addition to the electrostatic interactions in the lateral grooves, π-π interactions occurs between the R9 ligand and the nitrogenous bases. This happens because R9 is an aromatic molecule capable of stacking between the guanine tetrads characteristic of the G-quadruplex. This stacking increases structural stability by enhancing conjugation and delocalizing π electrons. As a result, the energy required for electronic transitions decreases, causing a shift towards longer wavelengths. Notably, the same π-π interactions also occurs in other forms of DNA, such as duplex, where the nitrogenous bases facilitate aromatic stacking with the R9 ligand. The duplex is associated with H28, and in the case of IDJ1 at pH 7, it has a part of i-motif and another part of duplex, with the interaction with R9 being specific to the duplex region.

6.3. CIRCULAR DICHROISM SPECTROSCOPY

Circular dichroism spectroscopy may reveal conformational changes in DNA structures upon interaction with the R9 ligand. In the circular dichroism instrument, several experiments were performed to obtain information of various types. First, CD spectra of solutions of DNA and DNA with R9 were measured, with their concentrations presented in the Experimental Procedure section.

Figure 11 shows the spectrum of both Pu22T14T23 and TBA, as both structures are G-quadruplexes. Pu22T14T23 is parallel, while TBA is antiparallel. It can be observed that the parallel structure has a positive peak at 260 nm, whereas the antiparallel structure has it at 290 nm. Also, negative signals at 240 nm for Pu22T14T23 and at 260 nm for TBA were observed. It should be noted that the positive signals are twice as high as the negative signals.

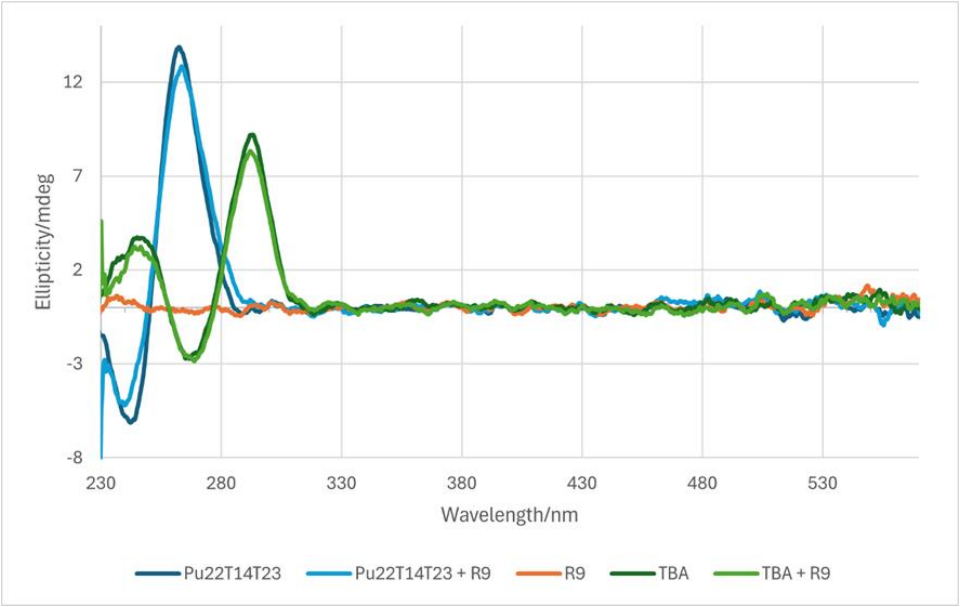

Figure 11: Ellipticity *vs.* Wavelength of DNA samples. DNA and dye concentrations were 2 and 6 micromolar, respectively. Measurements done at 20 ºC.

These characteristics of the G-quadruplex can be explained by the fact that guanines are responsible for light absorption in the UV-Vis spectrum region with wavelength greater than 210 nm. Guanines have two significant absorption bands between 240 and 290 nm, due to specific electronic transitions corresponding to π-π transitions [19]. These transitions are oriented differently, one aligned along the short axis of the molecule and the other along the long axis. This explains why the positive peak is twice as high as the negative peak, as the geometry can typically favour an orientation that amplifies one of the bands. Positive peaks are generated due to the stacking of two G-quartets with the same orientation in their hydrogen bonds, while negative peaks result from the stacking of two G-quartets with opposite orientation in their hydrogen bonds. The guanine tetrads stack on top of each other with a certain rotation, causing the transition dipole moments of the guanines to interact with each other. This interaction, known as chiral exciton coupling, generates specific patterns in the CD spectra. [20]

The presence of the R9 ligand causes a slight decrease in the intensity of the bands. In the case of Pu22T14T23, this decrease is observed in both the positive and negative peaks, whereas in the case of TBA, only the positive band shows a decrease. This behaviour may indicate a small change in the conformation of the TBA-R9 complex.

In Figure 12, the H28, which corresponds to a duplex structure, shows a positive peak at 270 nm and a negative peak at 240 nm, both with similar intensities. For the IDJ1, which corresponds to a duplex/i-motif hybrid structure at pH 7, there is a positive signal at 270 nm and a less intense negative signal at 240 nm. The temperature of this measurement was set at 15 ºC because if the temperature had been higher, the i-motif structure would no longer be present.

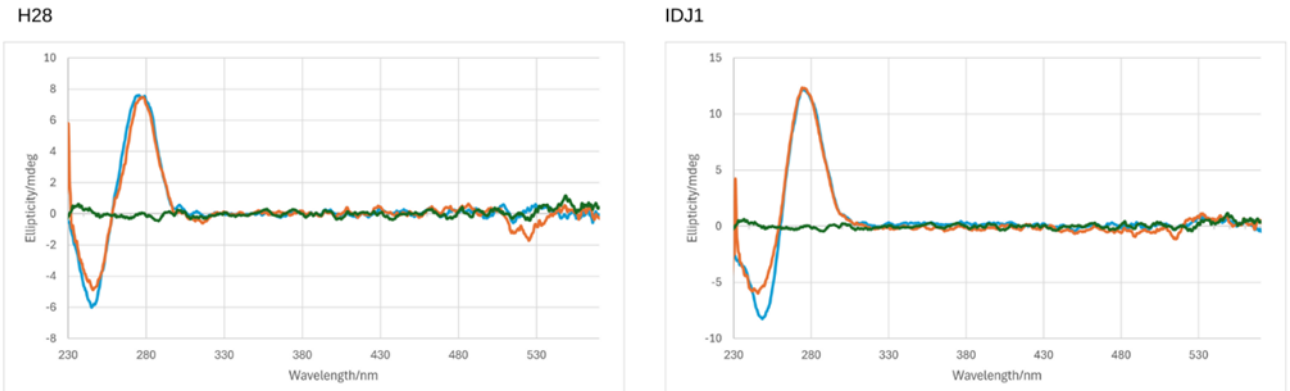

Figure 12: Ellipticity *vs.* Wavelength of DNA samples. DNA and dye concentrations were 2 and 6 micromolar, respectively. Measurements done at 20 ºC.

In these two cases, the presence of the R9 ligand causes a decrease in the negative band, without any change observed in the positive peak. This does not provide clear information about a conformational change in the complex. However, the signal change in the 450-600 nm range does.

The R9 ligand, being an achiral molecule, does not exhibit an intrinsic CD spectrum. However, its interaction with DNA causes a slight reduction in signal intensity in the 240-300 nm range, except in the case of T25. Simultaneously, a signal appears in the 450-600 nm range, which has been detected in Pu22T14T23 and H28. It is possible that a signal is also present in the other DNA samples, but in our results, it is not clearly visible. This decreases in signal indicates changes in chirality, suggesting the intercalation of small molecules, such as the ligand itself. Subsequently, titrations of DNAs with R9 ligands were carried out to analyse this observed signal in detail.

The experimental procedure executed for the titrations was already described in the Experimental Procedure section. These titrations were performed only for Pu22T14T23 and H28, selected for having the most prominent signals. Below are the Figure 13 and Figure 14 with the spectra, accompanied by a colour bar illustrating the changes associated with increasing ligand concentration. The graph shows an increase in the signal in the 450-600 nm range, allowing the analysis of R9's behaviour when interacting with DNA.

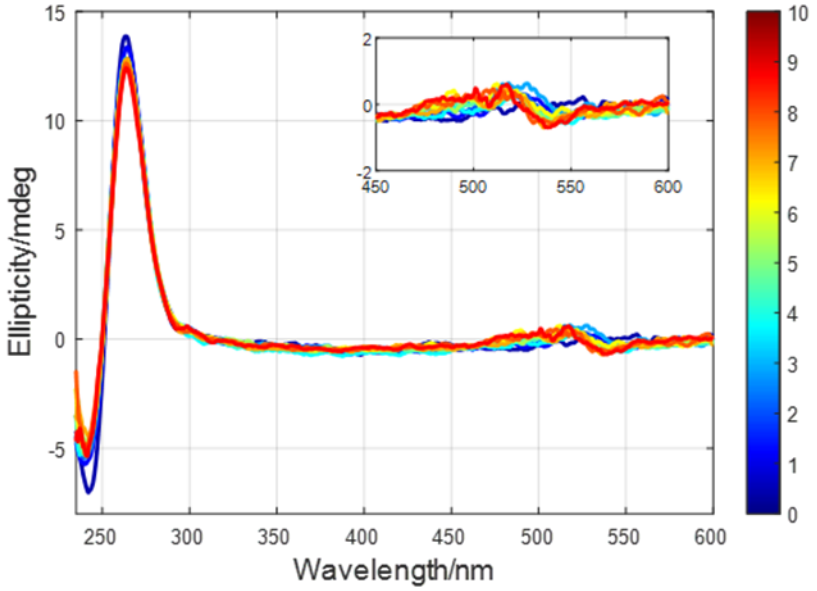

Figure 13: Ellipticity *vs*. Wavelength of titration of sample Pu22T14T23 with R9. Initial DNA concentration was 2 micromolar. Numbers in the colour bar indicate the changes associated with increasing ligand R9 concentration. The temperature was set to 20 ºC.

For Pu22T14T23, two slight peaks, one positive and one negative, are observed, indicating the presence of chiral excitation coupling [21]. This phenomenon suggests that the ligand has not only bound to the DNA, but possibly stacked on its exterior. This is evidenced by the formation of a signal that would not appear if the molecule were completely symmetrical.

On the other hand, the spectrum of H28 shows a strong negative signal that intensifies as the ligand concentration increases (Figure 14). This type of signal indicates that the ligand has intercalated between the strands of the duplex, partially preserving the symmetry of the structure [21]. The absence of a positive induced CD peak reinforces the idea that there are no complex interactions or significant stacking of dye molecules, as these typically generate characteristic exciton peaks.

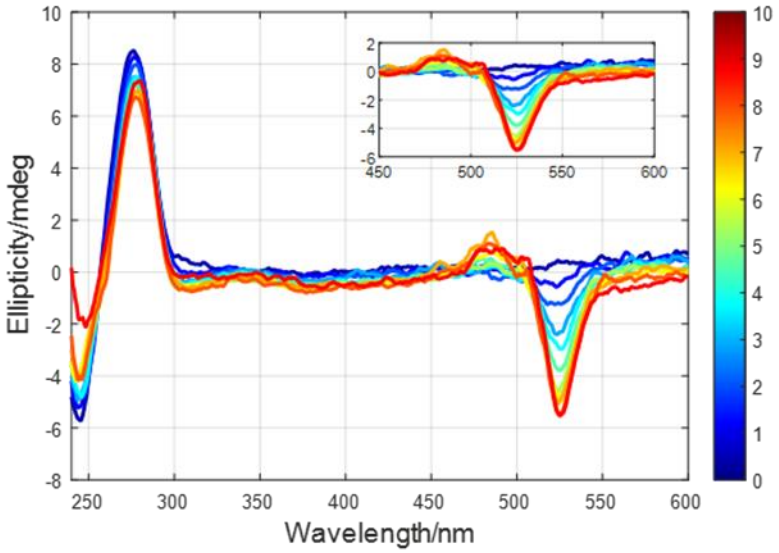

Figure 14: Ellipticity *vs*. Wavelength of titration of sample H28 with R9. Initial DNA concentration was 2 micromolar. Numbers in the colour bar indicate the changes associated with increasing ligand R9 concentration. The temperature was set to 20 ºC.

After analysing the spectra of the different structures and observing the signal change induced by the R9 ligand, it was decided to investigate the effect of the ligand on the molecule denaturation. The experimental procedure and temperature conditions used during the measurements are detailed in section 5.2.3. These denaturation processes were carried out for the DNAs Pu22T14T23, H28, QDJ1, and IDJ1.

Figure 15 illustrates the behaviour of the Pu22T14T23 complex both without and with the R9 as the temperature increases. The colour bar in the graph represents this gradual temperature rise. It is clearly observed that the intensity of the peaks progressively decreases as the temperature rises. In the case of Pu22T14T23 without R9, the loss of structure is significantly greater compared to the complex with the ligand. This phenomenon is explained by the denaturation of Pu22T14T23, which initially adopts a G-quadruplex structure but loses its ordered configuration and transforms into a single-stranded DNA. The presence of the R9 ligand mitigates this structural loss, showing how it influences the denaturation process.

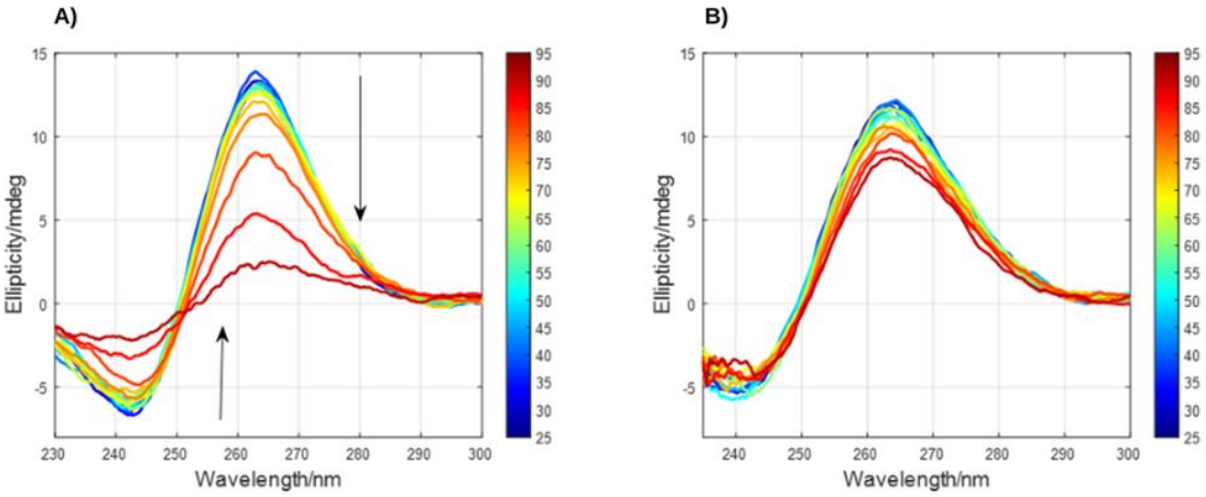

Figure 15: Thermal denaturation of (A) Pu22T14T23 and (B) Pu22T14T23 with R9. DNA concentration was 2 micromolar in both cases and R9 concentration was 6 micromolar.

This result shows how the G-quadruplex loses its structural stability when subjected to very high temperatures and highlights the protective role of R9. This same denaturation phenomenon is also observed in other DNA structures, such as the duplex, i-motif, and hairpin.

To delve deeper into the loss or gain of structural stability of the different DNA structures, spectral data were analysed to determine the melting temperature (T_m) at the wavelength where ellipticity reached its maximum value. For this purpose, the sigmoidal function equation was used, which allows for the interpretation of the melting temperature (T_m).

The melting temperature (Tm) indicates the point where 50% of the structure is denatured, while the other 50% remains intact.

In Figure 16, the denaturation graphs of Pu22T14T23 and Pu22T14T23 with R9 are shown, along with the fitted sigmoidal curve of DNA.

- Blue curve: The T_m is 88.6 ± 0.8 ºC, where there is a sharp drop in ellipticity. This indicates that this G-quadruplex structure is very stable under biological conditions of temperature (37 ºC).
- Red curve: The T_m occurs at an even higher temperature than in the blue curve. This suggests that the presence of the R9 ligand increases the thermal stability of the G-quadruplex, requiring a higher temperature to induce its denaturation.

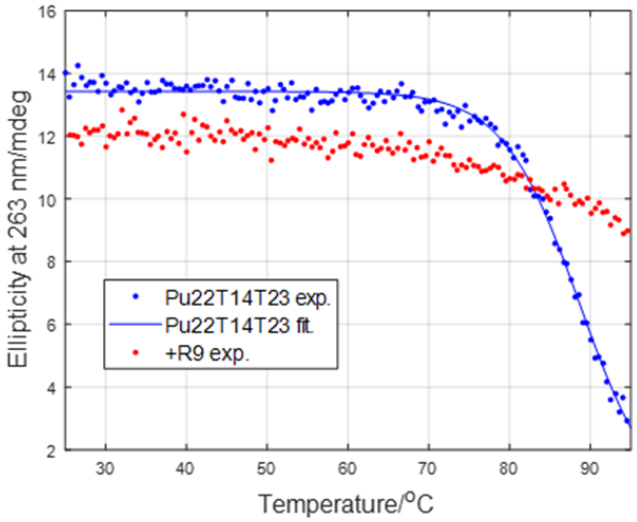

Figure 16: Melting curve at 263 nm of Pu22T14T23 samples.

Table 4 presents the melting temperature (T_m) of the different DNA structures, both in the absence and presence of the R9 ligand, as well as the observed differences between both cases.

Table 4: Melting temperatures of DNA samples and DNA samples with R9 and the value of ΔT_m in relation to the difference between the Tm with and without R9.

DNA		**T_m (ºC)**		
		DNA	DNA + R9	ΔT_m
Pu22T14T23		88.6±0.8	>95	-
H28		68.0±0.5	70.3±0.6	2.3±1.1
QDJ1		58.1±0.5	64.7±0.7	6.6±1.2
IDJ1	T_{m1}	15.2±0.4	11.9±0.9	-3.3±1.3
	T_{m2}	73.2±10	n.d	-

It is noteworthy that the T_m of Pu22T14T23, with or without R9, is significantly higher compared to the other analysed DNA structures. This can be attributed to the presence of the G-quadruplex structure, characterized by the formation of guanine tetrads that provide remarkable thermal stability.

On the other hand, H28 and QDJ1 have similar T_m values despite their structural differences: H28 corresponds to a duplex structure, while QDJ1 is classified as an antiparallel G-quadruplex with an additional hairpin. The lower T_m of QDJ1 compared to Pu22T14T23 can be explained by the fact that Pu22T14T23 has three tetrads, whereas QDJ1 only has two. This causes QDJ1 to denature earlier as it is not as stable as Pu22T14T23.

For IDJ1, two T_m values are observed, reflecting the coexistence of two distinct structures: an i-motif and a hairpin [19]. The first thermal transition (T_{m1}) corresponds to the denaturation of the i-motif, which is not very stable at pH 7 because a small fraction of cytosines is protonated. The second transition (T_{m2}) has been assigned to the denaturation of the hairpin.

Finally, it is important to note that, the presence of the R9 ligand increases the melting temperatures, indicating an increase in the thermal stability of the DNA structures. However, this pattern does not hold for IDJ1. This finding reinforces the hypothesis that R9 plays a stabilizing role in most structures.

With this information, we can conclude that there is an interaction between the DNA and the ligand, which was also observed at the beginning of the study through fluorescence. At that point, it was determined that an increase in fluorescence indicated the formation of the DNA-R9 complex.

6.4. HIGH-PERFORMANCE LIQUID CHROMATOGRAPHY

Several tests were conducted to set up the HPLC instrument, as detailed in the Experimental Procedure section. These tests did not have a specific objective or hypothesis related to DNA and the ligand; the main purpose was to study and understand the instrument's performance and get knowledge on Empower software. Nevertheless, additional information was sought to identify the optimal conditions for testing DNA samples.

Measurements were ultimately performed using a mobile phase consisting of 0.1 M triethylammonium acetate (phase A) and acetonitrile (phase B) in a 60:40 ratio. The column operated under isocratic conditions with a flow rate of 0.25 mL/min. A chromatogram of Pu22T14T23 (Figure 17) is provided to demonstrate that the instrument is operating properly, offering insight into peak retention time and absorbance.

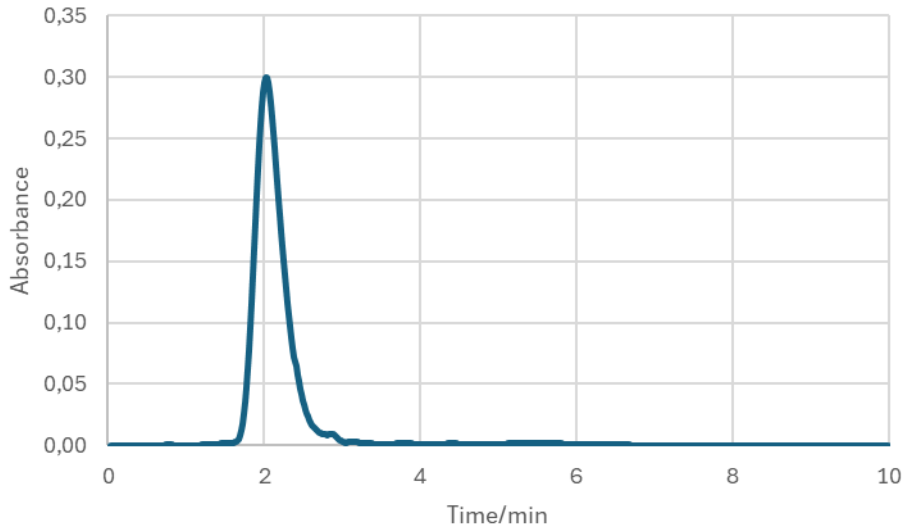

Figure 17: Chromatogram of Pu22T14T23, with a mobile phase composed of phase A (TEAA 0.1 M) and phase B (ACN) in a 60:40 ratio.

Figure 18 displays the retention times and the number of nucleotides for each DNA samples. The results indicate that the retention time and length of DNA strand follow a linear relationship, though no conclusive information could be determined regarding the precise elution order of the samples from the column.

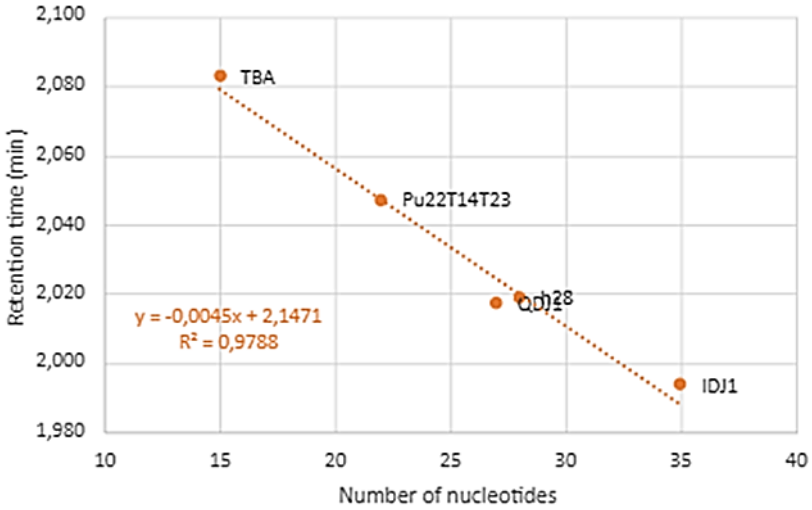

Figure 18: Retention time *vs*. number of nucleotides of DNA samples.

However, after testing, it was concluded that the available C18 reverse-phase column was not the most suitable choice for this type of analysis, as it failed to provide the desired information about the effect of the different folding of DNA structures on the retention time.

A more appropriate alternative could be size exclusion chromatography (SEC), which separates particles based on their size. This approach would have been ideal, as it minimizes interactions between the sample and both the mobile and stationary phases, yielding more relevant data for the DNA structure analysed.

10. CONCLUSIONS

The main objective of this project has been to study the interaction of the fluorescent ligand R9 with different DNA structures using a variety of experimental techniques. The results obtained allow the following conclusions to be drawn:

1. Interaction of the R9 ligand with DNA
    - Fluorescence spectroscopy measurements confirm that the R9 ligand interacts with DNA structures, although the intensity of interactions varies depending on the specific structure analysed. The interaction is particularly significant in the case of the G-quadruplex Pu22T14T23, as reflected by the higher fluorescence intensity.
    - UV-Vis absorption spectra provide clear indicators of molecular interaction, such as hypochromic shifts (reduction in absorption intensity), which indicate the formation of DNA-ligand complexes. Additionally, bathochromic shifts (wavelength shifts toward longer values) suggest changes in the electronic environment when the ligand binds to DNA.
    - In G-quadruplex, the main interaction involves π-π interactions between stacked nitrogenous bases and the aromatic ligand, along with electrostatic interactions between the DNA phosphate groups and the ligand's amines. In unstacked structures such as T25, the interaction is exclusively due to electrostatic forces, given the absence of base stacking.
2. Structural effects induced by R9
    - Circular dichroism (CD) spectra show that the interaction of the R9 ligand induces structural modifications in some DNA structures. In the case of the G-quadruplex Pu22T14T23, a phenomenon known as chiral exciton coupling is observed, indicating that ligand binds externally. In contrast, in the duplex DNA H28, the ligand intercalates between the strands.
    - Thermal denaturation experiments reveal that R9 increases the thermal stability of DNA structures. This phenomenon is evidenced by the Tm values, where an increase indicates greater thermal stability.

In summary, this project has contributed to the search for ligands capable of stabilizing non-canonical DNA structures, such as G-quadruplex found at telomeric ends. These structures are key to regulating telomerase, an enzyme active in most cancers. The ability of R9 to stabilize G-quadruplex makes it a promising tool for further studies on the replication of the 3' end of telomeric DNA and its potential relationship with cancer development.

11. REFERENCES AND NOTES

[1] J. Carlos García-Ramos, R. Galindo-Murillo, F. Cortés-Guzmán, and L. Ruiz-Azuara, "Metal-Based Drug-DNA Interactions," *Chem. Soc*, vol. 57, no. 3, pp. 245–259, Jun. 2013.

[2] J. D. Watson and F. H. C. Crick, "A structure for deoxyribose nucleic acid. 1953," *Nature (London)*, vol. 421, no. 6921, pp. 397–8, Jan. 2003.

[3] V. A. Bloomfield, D. M. Crothers, I. Tinoco, and J. E. Hearst, *Nucleic acids: structures, properties, and functions*. Sausalito, California, 2000.

[4] A. I. Karsisiotis, C. O'Kane, and M. Webba da Silva, "DNA quadruplex folding formalism - A tutorial on quadruplex topologies," *Methods*, vol. 64, no. 1, pp. 28–35, Nov. 2013, doi: 10.1016/j.ymeth.2013.06.004.

[5] E. Largy, V. Gabelica, and J.-L. Mergny, "Basics of G-quadruplex structures A quick overview of the (nucleo)bases of G-quadruplex nucleic acids." Accessed: Jan. 12, 2024. [Online]. Available: https://ericlarg4.github.io/Distill_section/docs/guideline.html

[6] S. Burge, G. N. Parkinson, P. Hazel, A. K. Todd, and S. Neidle, "Quadruplex DNA: Sequence, topology and structure," *Nucleic Acids Res*, vol. 34, no. 19, pp. 5402–5415, Nov. 2006, doi: 10.1093/nar/gkl655.

[7] J. Spiegel, S. Adhikari, and S. Balasubramanian, "The Structure and Function of DNA G-Quadruplexes," Feb. 01, 2020, *Cell Press*. doi: 10.1016/j.trechm.2019.07.002.

[8] N. Maizels and L. T. Gray, "The G4 Genome," *PLoS Genet*, vol. 9, no. 4, Apr. 2013, doi: 10.1371/journal.pgen.1003468.

[9] S. Benabou, A. Aviñó, R. Eritja, C. González, and R. Gargallo, "Fundamental aspects of the nucleic acid i-motif structures," 2014, *Royal Society of Chemistry*. doi: 10.1039/c4ra02129k.

[10] A. S. Gouda, M. S. Amine, and E. B. Pedersen, "Improved i-motif thermal stability by insertion of anthraquinone monomers," *Org Biomol Chem*, vol. 15, no. 31, pp. 6613–6621, 2017, doi: 10.1039/c7ob01393k.

[11] J. Rodriguez *et al.*, "Exploring the stabilizing effect on the i-motif of neighboring structural motifs and drugs," *Int J Biol Macromol*, vol. 242, Jul. 2023, doi: 10.1016/j.ijbiomac.2023.124794.

[12] J. Choi and T. Majima, "Conformational changes of non-B DNA," *Chem Soc Rev*, vol. 40, no. 12, pp. 5893–5909, Nov. 2011, doi: 10.1039/c1cs15153c.

[13] D. Bikard, C. Loot, Z. Baharoglu, and D. Mazel, "Folded DNA in Action: Hairpin Formation and Biological Functions in Prokaryotes," *Microbiology and Molecular Biology Reviews*, vol. 74, no. 4, pp. 570–588, Dec. 2010, doi: 10.1128/mmbr.00026-10.

[14] N. Ishkitiev *et al.*, "Nanoconfined Chlorine-Substituted Monomethine Cyanine Dye with a Propionamide Function Based on the Thiazole Orange Scaffold—Use of a Fluorogenic Probe for Cell Staining and Nucleic Acid Visualization," *Molecules*, vol. 29, no. 24, p. 6038, Dec. 2024, doi: 10.3390/molecules29246038.

[15] N. Ishkitiev *et al.*, "Aggregation induced nucleic acids recognition by homodimeric asymmetric monomethyne cyanine fluorochromes in mesenchymal stem cells," *Int J Biol Macromol*, vol. 250, p. 126094, Oct. 2023, doi: 10.1016/j.ijbiomac.2023.126094.

[16] J. Kypr, I. Kejnovská, D. Renčiuk, and M. Vorlíčková, "Circular dichroism and conformational polymorphism of DNA," 2009. doi: 10.1093/nar/gkp026.

[17] Waters, "Atlantis T3, DC18 and HILIC silica columns."

[18] C. Poyato, J. Pacheco, A. Domínguez, R. Eritja, A. Aviñó, and R. Gargallo, "Assessment of methodologies based on the formation of antiparallel triplex DNA structures and fluorescent silver nanoclusters for the detection of pyrimidine-rich sequences," *Spectrochim Acta A Mol Biomol Spectrosc*, vol. 329, p. 125567, Mar. 2025, doi: 10.1016/j.saa.2024.125567.

[19] S. Masiero *et al.*, "A non-empirical chromophoric interpretation of CD spectra of DNA G-quadruplex structures," *Org Biomol Chem*, vol. 8, no. 12, p. 2683, 2010, doi: 10.1039/c003428b.

[20] P. L. T. Tran, J. L. Mergny, and P. Alberti, "Stability of telomeric G-quadruplexes," *Nucleic Acids Res*, vol. 39, no. 8, pp. 3282–3294, 2011, doi: 10.1093/nar/gkq1292.

[21] E. W. White *et al.*, "Structure-specific recognition of quadruplex DNA by organic cations: Influence of shape, substituents and charge," *Biophys Chem*, vol. 126, no. 1–3, pp. 140–153, Mar. 2007, doi: 10.1016/j.bpc.2006.06.006.

[22] I. Serrano Chacón "Combinando motivos canónicos y no canónicos del ADN: estructura, dinámica y reconocimiento molecular," Universidad Complutense, Madrid, 2021.

[23] I. Serrano-Chacón, B. Mir, N. Escaja, and C. González, "Structure of i-Motif/Duplex Junctions at Neutral pH," *J Am Chem Soc*, vol. 143, no. 33, pp. 12919–12923, Aug. 2021, doi: 10.1021/jacs.1c04679.

12. ACRONYMS

A: Adenine

C: Cytosine

CD: Circular Dichroism

DNA: Deoxyribonucleic acid

dsDNA: Double-stranded DNA

G: Guanine

HPLC: High-Performance Liquid Chromatography

R9: (E)-1-(3-amino-3-oxopropyl)-4-((3-(3-(3-(3-(pyridin-1-io-1-yl)propyl)venzo[d]thiazol-2(3H)-ylidene)methyl)quinolin-1-io diiodide

RNA: Ribonucleic acid

ssDNA: Single-stranded DNA

T: Thymine

TEAA: triethylamine acetate

Tm: melting temperature

UV-Vis: Ultraviolet/Visible

APPENDICES

APPENDIX 1: MOLECULAR ABSORPTION SPECTROSCOPY

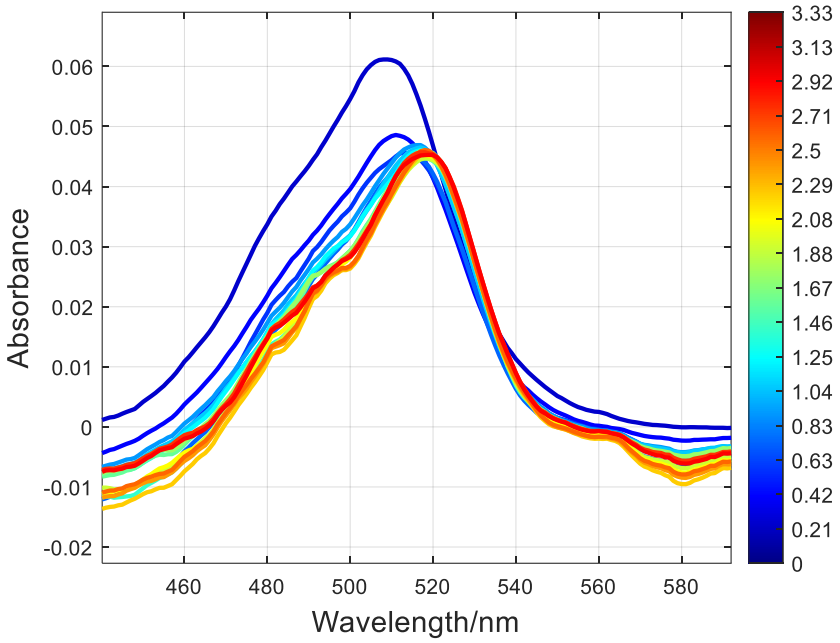

Figure 1: Absorbance *vs.* Wavelength of titration of H28 with R9. Initial R9 concentration was 1.5 micromolar. Experiment carried out at 20 ºC. Numbers at the colour bar indicate the changes associated with increasing DNA concentration.

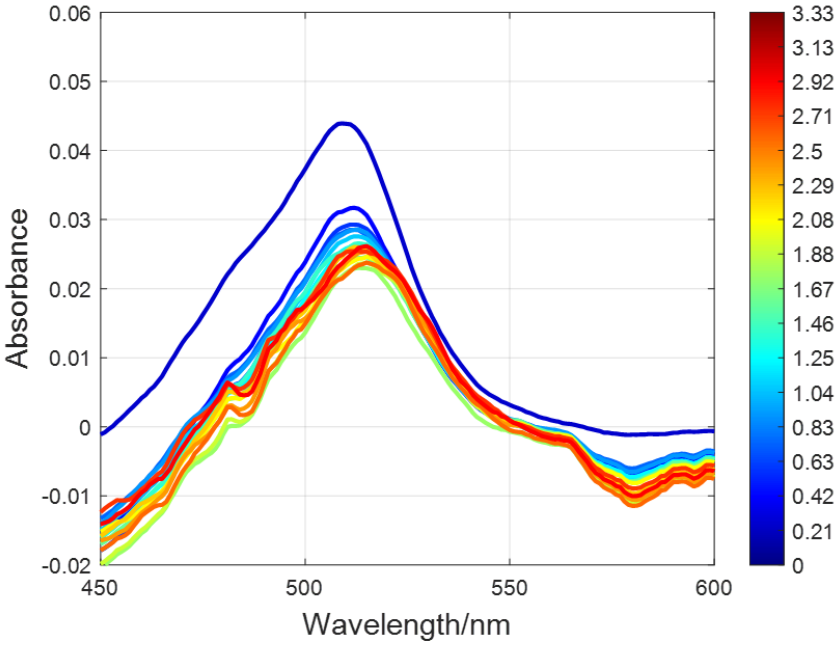

Figure 2: Absorbance *vs.* Wavelength of titration of TBA with R9. Initial R9 concentration was 1.5 micromolar. Experiment carried out at 20 ºC. Numbers at the colour bar indicate the changes associated with increasing DNA concentration.

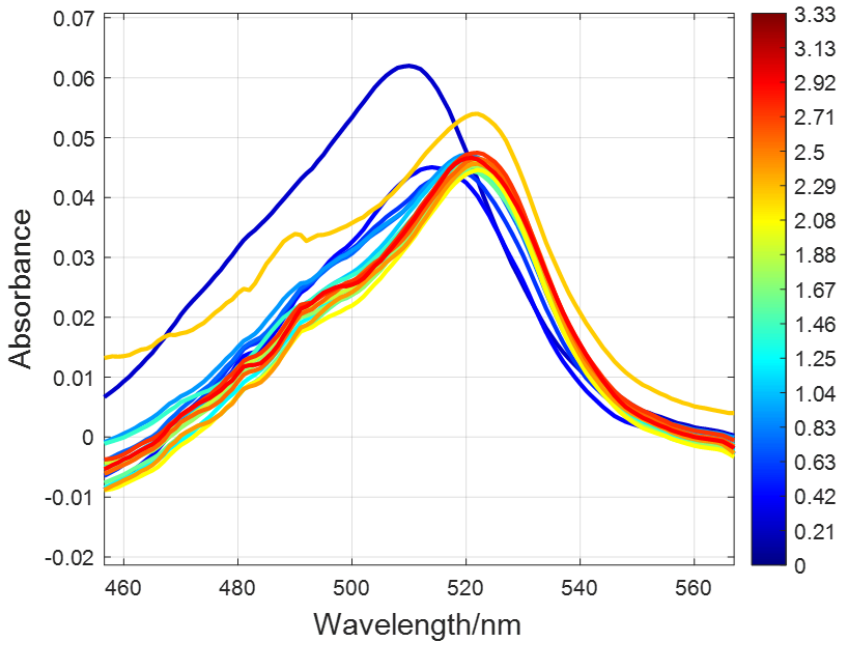

Figure 3: Absorbance *vs.* Wavelength of titration of QDJ1 with R9. Initial R9 concentration was 1.5 micromolar. Experiment carried out at 20 ºC. Numbers at the colour bar indicate the changes associated with increasing DNA concentration.

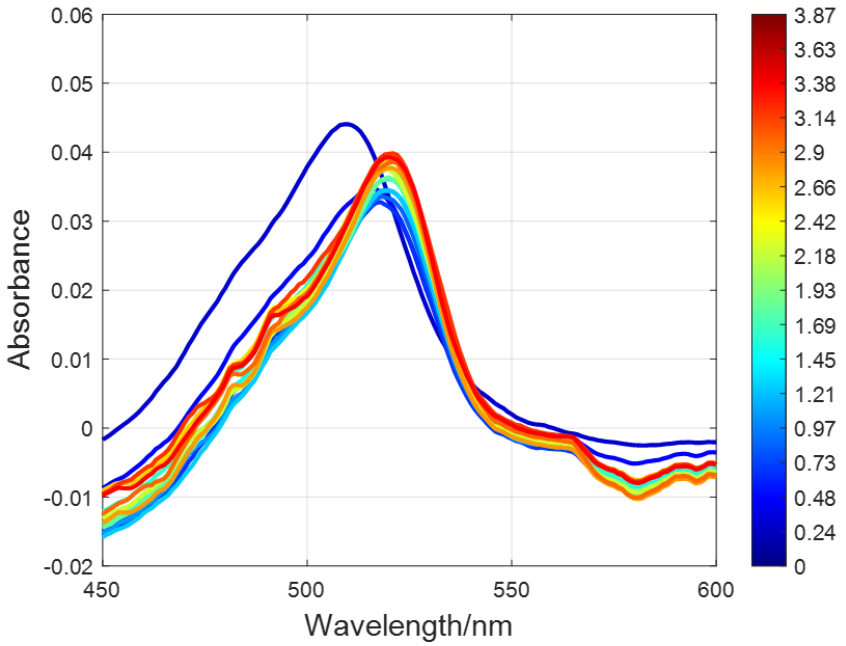

Figure 4: Absorbance *vs.* Wavelength of titration of IDJ1 with R9. Initial R9 concentration was 1.5 micromolar. Experiment carried out at 20 ºC. Numbers at the colour bar indicate the changes associated with increasing DNA concentration.

APPENDIX 2: CIRCULAR DICHROISM SPECTROSCOPY

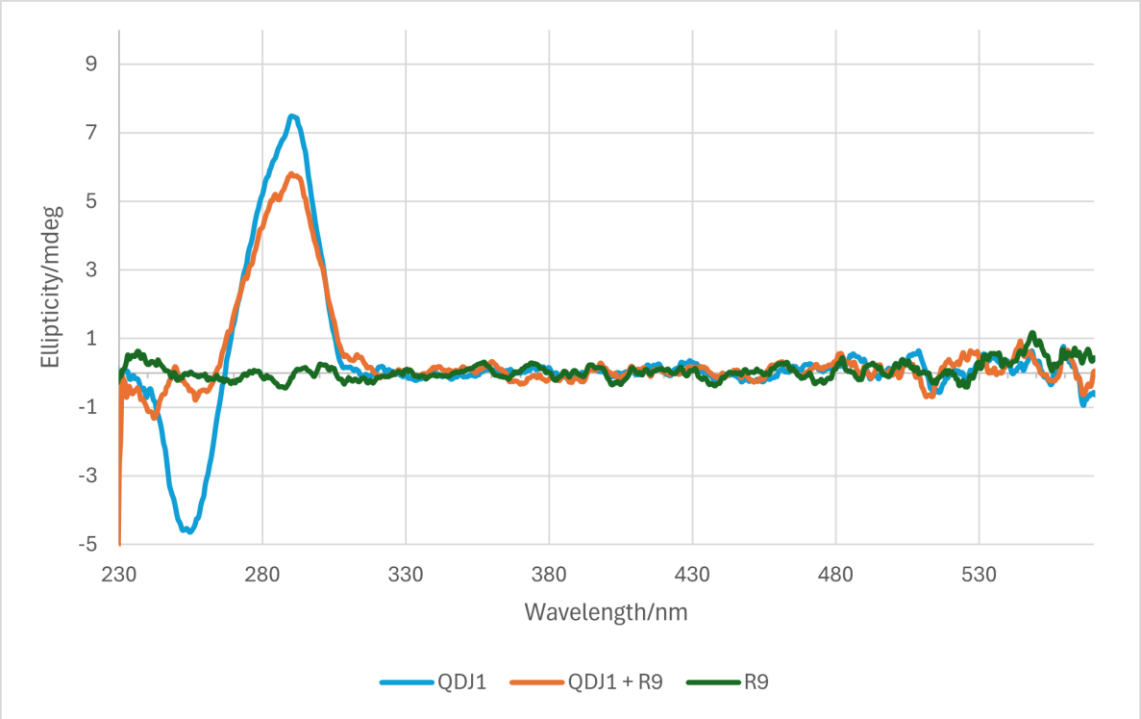

Figure 5: Ellipticity vs. Wavelength of QDJ1. DNA and dye concentrations were 2 and 6 micromolar, respectively. Measurements done at 20 ºC.

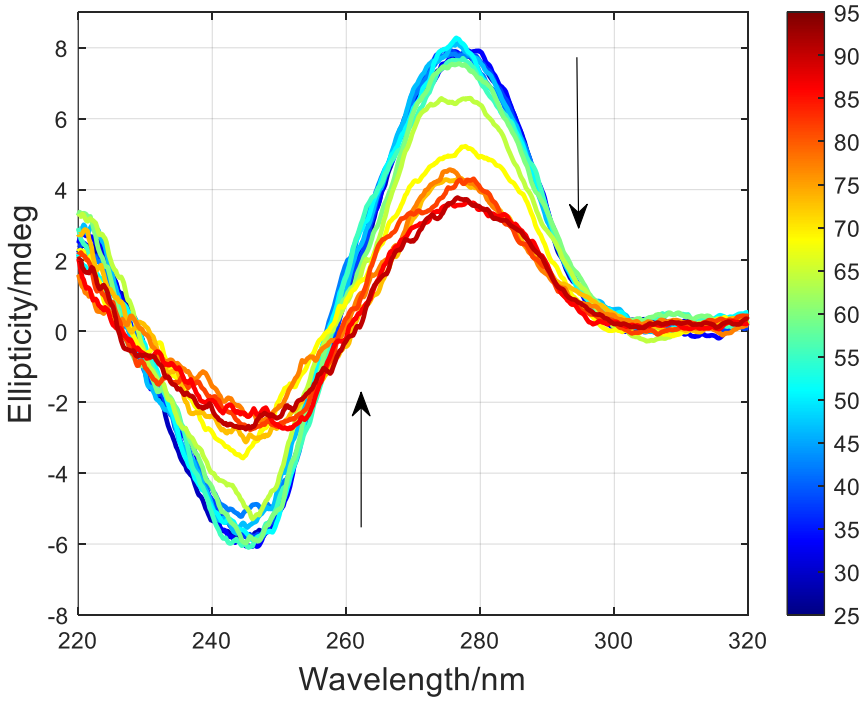

Figure 6: Thermal denaturation of H28. DNA concentration was 2 micromolar.

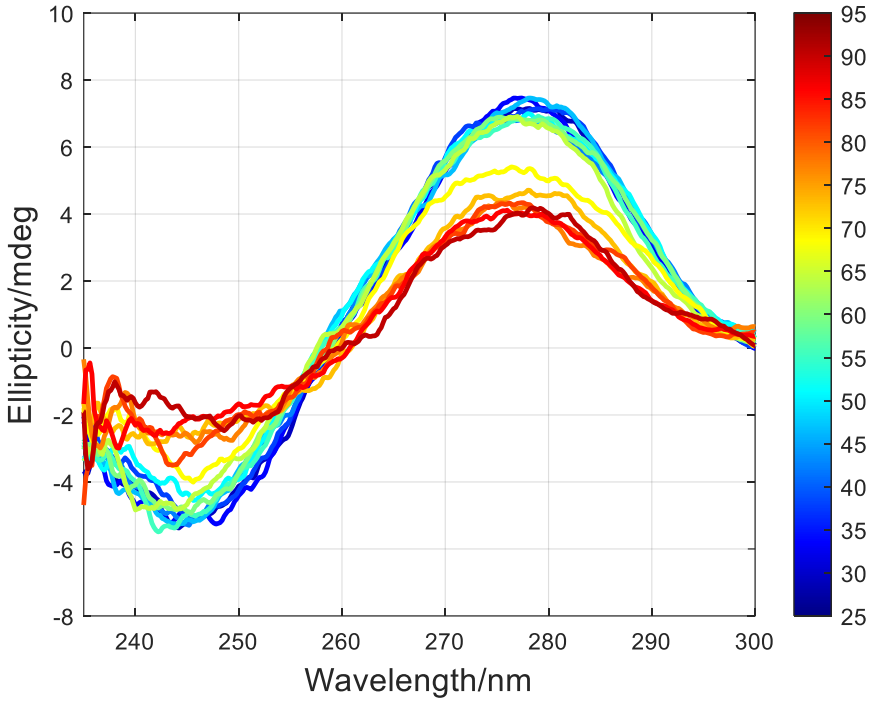

Figure 7: Thermal denaturation of H28 with R9. DNA and dye concentrations were 2 and 6 micromolar, respectively.

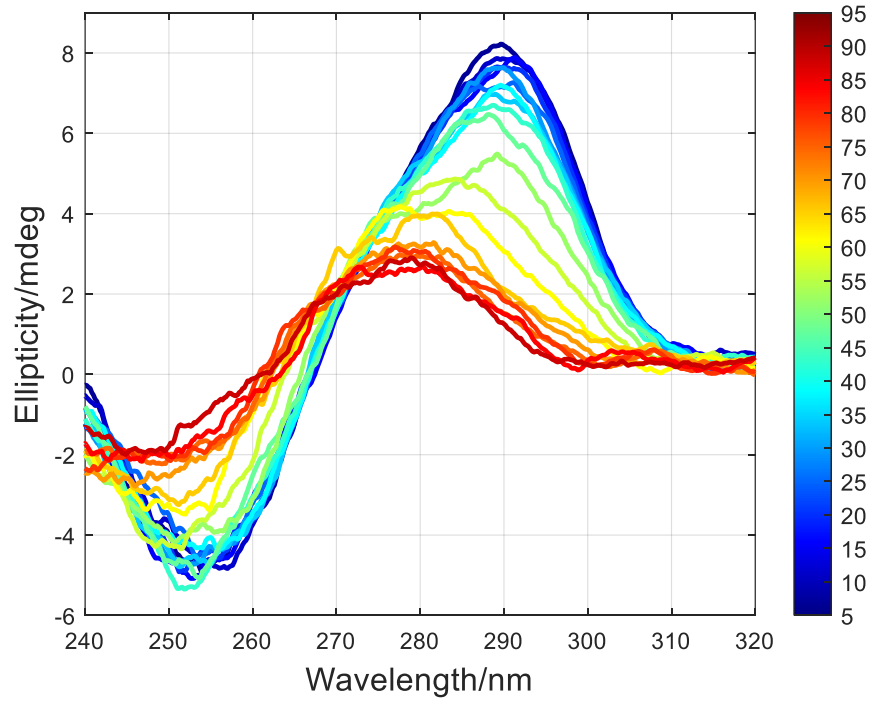

Figure 8: Thermal denaturation of QDJ1. DNA concentration was 2 micromolar.

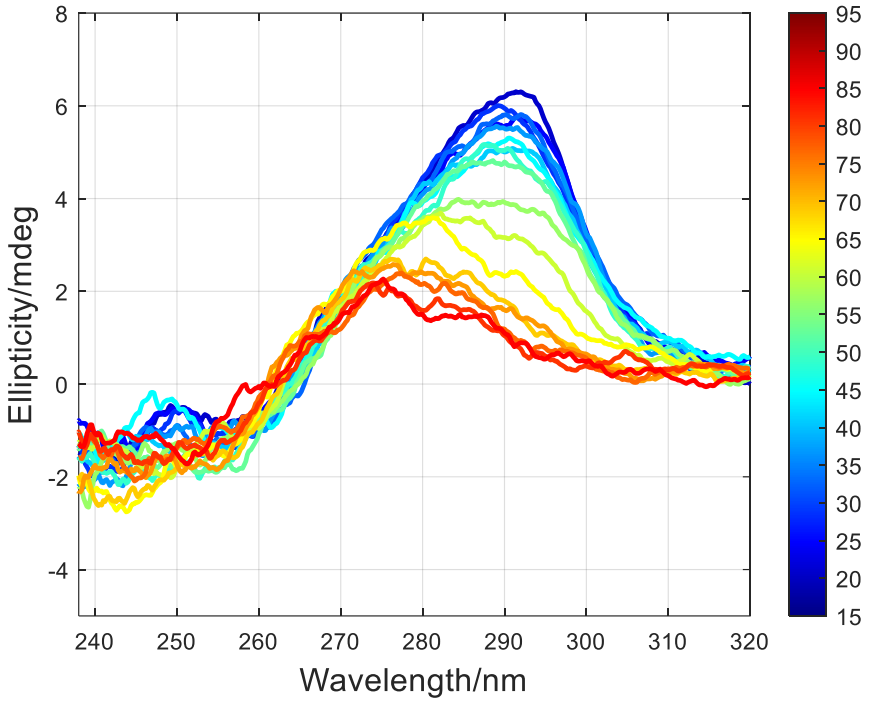

Figure 9: Thermal denaturation of QDJ1 with R9. DNA and dye concentrations were 2 and 6 micromolar, respectively.

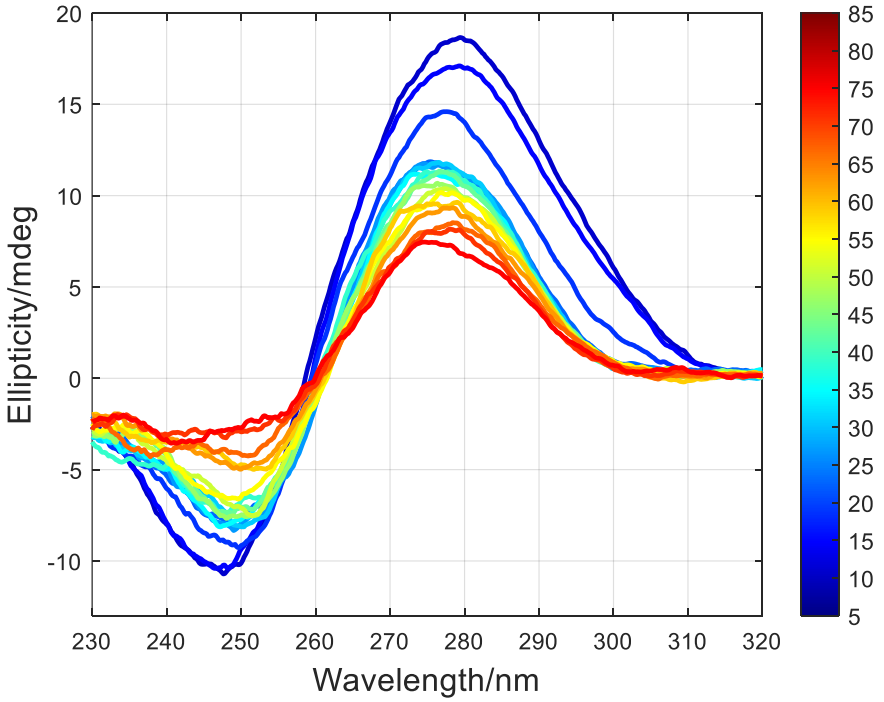

Figure 10: Thermal denaturation of IDJ1. DNA concentration was 2 micromolar.

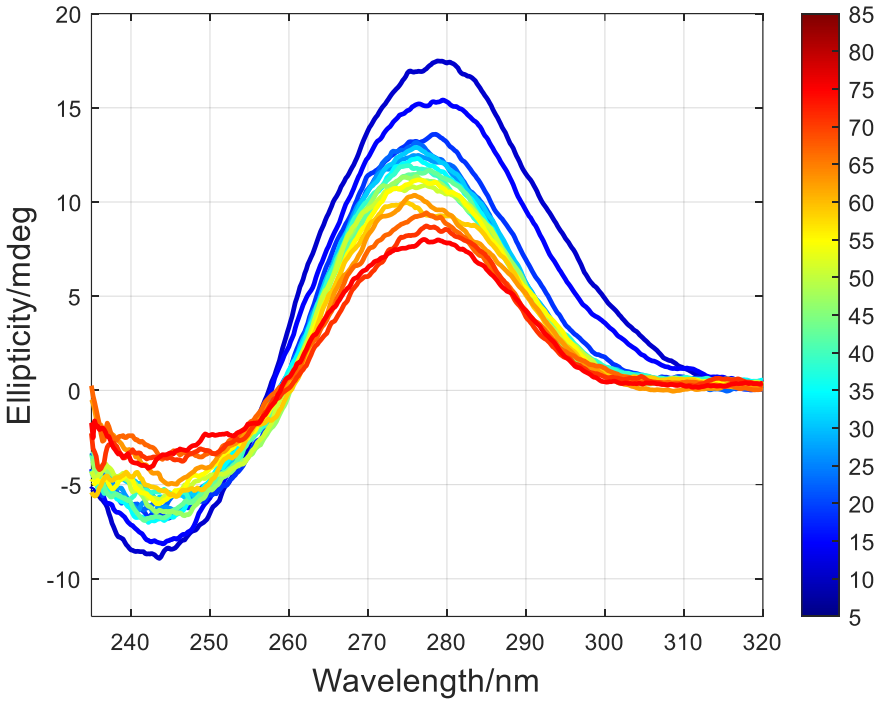

Figure 11: Thermal denaturation of IDJ1 with R9. DNA and dye concentrations were 2 and 6 micromolar, respectively.